EMI Conducted Emission on Synchronization Conditions for FPGA-Based Multidrives Network

1st Douglas Nascimento*
University of Zielona Góra
University of Twente
Hitachi Energy
Kraków, Poland
eng.douglas.a@ieee.org

2nd Robert Smoleński
Institute of Automatic Control,
Electronics and Electrical Engineering
University of Zielona Góra
Zielona Góra, Poland
r.smolenski@iee.uz.zgora.pl

3rd Piotr Leżyński
Institute of Automatic Control,
Electronics and Electrical Engineering
University of Zielona Góra
Zielona Góra, Poland
p.lezynski@iee.uz.zgora.pl

4th Michał Przybylski
Institute of Automatic Control,
Electronics and Electrical Engineering
University of Zielona Góra
Zielona Góra, Poland
m.przybylski@iee.uz.zgora.pl

5th Niek Moonen
University of Twente
Department of Power Electronics and
Electromagnetic Compatibility
Enschede, The Netherlands
niek.moonen@utwente.nl

Abstract—The power converters are essential for the development of renewable energy generation, conversion processes and energy storage systems. Besides, some applications require synchronization between converters e.g., industrial use as AC drives for motors, pumps, fans, drills and wheels. Thus, this paper presents a theoretical study with experimental validation of FPGA frequency and time synchronization conditions and its impact on conducted emissions (CE) from multidrives operations. For EMI assessment over those conditions, a LabVIEW-FPGA-based cyber-physical testbench was used to control the DC/AC converters using SPWM. It shows how the synchronization conditions impact the EMC in multiconverters systems over the EMI emissions and also highlights measures to mitigate the peak levels. The findings demonstrate that, depending on the condition, it reduces up to 29 dB of ground current peaks and 8 dB in EMI level, which may improve the EMC in DC distributed microgrids.

Index Terms—EMC, EMI, FPGA, AC Drives, waves superposition.

I. Introduction

The interactions on impedances between devices within the grid is well-known in literature and mainly occurs around the fundamental frequency of the supply voltage. It is considered in EMC requirements, that based on a deterministic statistics investigation, using impedance reference as IEC/TR 60725, the emission measurements on 2 - 9 kHz can be investigated as in the Informative Annex B to EN 61000-4-7:2002 [1]. Notwithstanding, below 150 kHz, the interactions between converter impedances, installation and loads need to be further assessed [1]–[3].

It is highlighted that the synchronization of switching operation may have an impact on the EMI measured [4], [5]. In spite of several studies have addressed CE of EMI in parallel multidrives systems [6]–[8], the literature review found no studies assessing EMI from the frequency and time

synchronization standpoint of FPGA controllers using SPWM modulation for multidrives application, which may constitute another improvement of EMC in DC distributed microgrids.

The contribution of this study relies on the investigation on the EMI impact of synchronization conditions provided by a cyber-physical system testbench using SPWM technique, which allows to control several AC drives with different switching frequencies. Thus, a comparison of the theory background based on analytical equations of geometrical model with experimental results is carried out. The analysis of the harmonics from multidrives network is provided in the range from CISPR-A band (9 - 150 kHz) and CISPR-B band ($150\,\text{kHz}$ - 30 MHz). Consequently, this study is particularly useful for those interested in distributed DC microgrid applications, variable speed drive (VSD)'s parameterization and EMI assessment of paralleled multiconverter systems.

Therefore, in Section II is presented the theoretical background on the conducted emission in VSDs. In Section IV-B is presented the methodology, testbench and reference EMI levels for a single VSD. In Section IV is shown the results from conducted emissions in parallel multidrive system. Finally, future studies and conclusion are dealt in Section V.

II. Conducted Emissions in PWM Converters

The phenomena behind the conducted disturbances in conventional electric drive systems are divided into common-mode and differential-mode emissions resulted from: the topology of inverter-based variable speed drive (mainly due star-type connection and parasitic components); the PWM waveform (i.e steep slopes with high dv/dt in trapezoidal shape waveform, ringing effects and to non-zero crosses); and resonances from impedance interactions from cables and other system components [9]–[12].

A. EMI from SPWM Switching Technique

In Si-based PWM converters working as AC drives, the EMI emissions are mostly presented in CISPR A band due
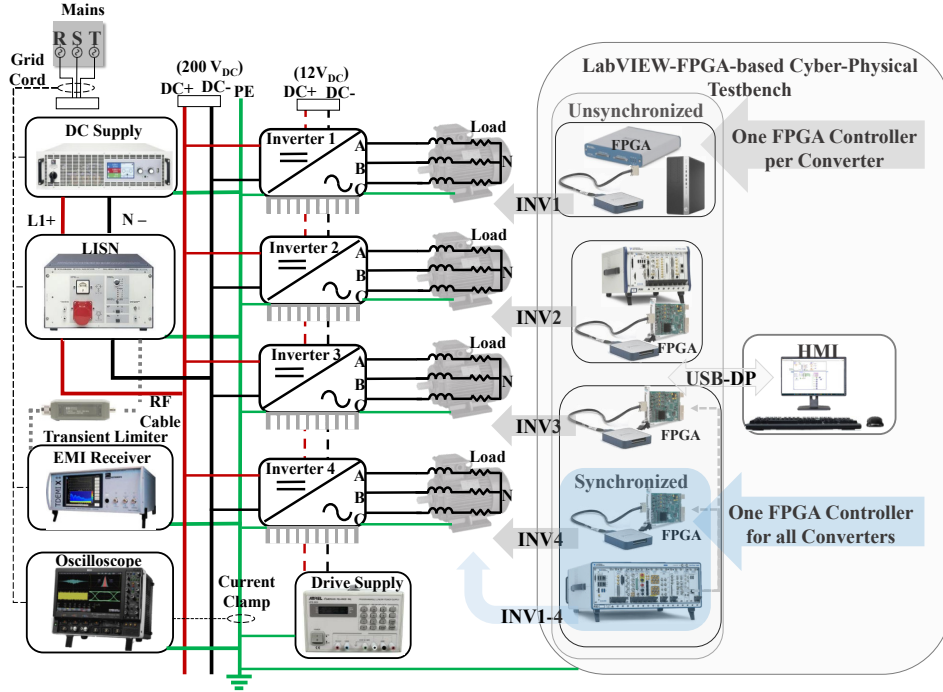
Fig. 1: Block diagram of connections.

to carrier frequency used over the controller [13]. For power converter modulated by SPWM, the emissions are ruled by the approximation given in (1) [14]:

$$u(t) \equiv MU_d \sin(\omega_s t)$$

$$+ 4\frac{U_d}{\pi} \sum_{m_1}^{\infty} \frac{J_n(\delta)}{m} \sin\frac{m}{2}\pi \cos(m\omega_c t)$$

$$+ 4\frac{U_d}{\pi} \sum_{m_2}^{\infty} \sum_{m_3}^{\pm\infty} \frac{J_n(\delta)}{m} \sin(\frac{m+n}{2}\pi)$$

$$\times \cos(m\omega_c t + n\omega_s t - \frac{n\pi}{2}) \quad (1)$$

where, $\delta = (mM\pi)/2$, $\omega_c = 2\pi f_c$, $\omega_s = 2\pi f_s$, $m_1 = 1, 3, 5, L$, $m_2 = 1, 2, L$, $m_3 = \pm1, \pm2, L$, U_d is the DC side voltage, M is the modulation factor, J_n is the Bessel function. However, in case of large differences in switching frequency between different devices, neglecting the value of switching frequency (f_c) and modulation frequency (f_s), and replacing it with m and n may be convenient. The value of m and n can be infinite in some circumstances, whereas emissions decrease as frequency increases. The spectrum follows the behavior observed by [14]: 1. Distribution at the f_c and its integer multiples, with magnitude reducing along with the frequency increasing. 2. Centered emissions levels on switching frequency and its integers, showing magnitude distributed symmetrically. 3. Furthermore, the emissions are multiple spaced of f_c, i.e. emissions ensue only when the frequency is $mf_c \pm nf_s$, for $m \in \mathbb{Z}^+$ and $n \in \mathbb{N}$.

B. EMI in Multiconverters Systems

Multiconverters systems emissions can be assessed by superposition of waves which can be done through complex numbers (or functions) by using either geometric progression

or phasor method, or by for summing of arithmetic sequences of cosines [15], [16]. This study presents the analysis of time and phase synchronization of switching pattern of parallel drives using the arithmetic summation of cosine functions, given two synchronization condition: synchronized and unsynchronized. Thus, the superposition of waves can be handled by summing arithmetic sequences. Using general cosine model for harmonic wave as in (2), where A is the wave amplitude, k is the wave number, represented by $k = 2\pi/\lambda$ (where λ is the wavelength), x is the position on the wave direction, ω is the angular frequency, t is the time and Θ_i is the initial phase, the explanation for waves superposition, of same amplitude is,

$$y_T(x,t) = A \sum_{i=1}^{N\to\infty} \cos(k_i x - \omega_i t + \Theta_i) \quad (2)$$

For positive integer N (number of converters) and real number R (synchronization state), the equations derived can be obtained based on the telescoping series [16]:

$$y_T(x,t) = A \sum_{i=1}^{N\to\infty} \cos(\omega_i t + \Theta_i)$$

$$= \begin{cases} NA\cos\omega t & , if \sin(\frac{1}{2}\Theta) = 0 \\ R\cos(\omega t + (N-1)\frac{1}{2}\Theta) & , otherwise \end{cases} \quad (3)$$

where the term $R \triangleq \sin(N\frac{1}{2}\Theta)/\sin(\frac{1}{2}\Theta)$, determines the synchronization state, in which $R = 1$ as synchronized and $R \neq 1$ as unsynchronized. The derivation of those equations can be found at [16], [17] and are useful to set the FPGA parameters for EMI tests.

III. FPGA-Based Cyber-physical System to Assess EMI in variable Speed Drives

The Fig. 1 shows the connections of EMI setup. The current study assesses EMI case studies of noise propagation in PWM

converters interactions. A FPGA-based cyber-physical system allows fast prototyping combined with industrial applications and support EMI assessment of power converters [18]. Thus, this study uses a FPGA-based testbench to provide reliable aggregated converters operation using SPWM switching technique. In the previous study [18], the EMI levels associated to SPWM parameterization for stand-alone operation were evaluated using this FPGA-based testbench. The system presented here, though, is an further extension providing the switching signals to multiple inverters to control machinery loads, with entire testbench assembled according to EN 61800-3 standard recommendations, following [7], [18], [19]. Herein the motors operate at no load condition.

In order to fully understand and keep signals unchanged, no EMI filters were applied to the system. The system provided three kinds of measurements: (1) frequency-domain and (2) time-frequency domain through LISN and EMI receiver and (3) time-domain measurement by current clamp connected to protective earth (PE) bus bar. Between the LISN and EMI receiver a transient limiter was added to protect the receiver. The EMI receiver provides a frequency range of 9 kHz - 6 GHz, following CISPR 16-2-1 with 200 Hz IFBW, for 9 - 150 kHz (CISPR-A), and 9 kHz IFBW, for 150 kHz - 30 MHz (CISPR-B). The devices specification shown in Table I.

TABLE I: Specification of devices used.

Device	Specification
Power Supply	EA-PSI 91500-30
LISN	R&S®ESH2-Z5 V-Network
Inverter	Powersys 80217 P3G 1000W
Controller Supply	Amrel LPS-305
EMI Receiver	Gauss TDEMI X6
3-Phase Induction Motor	1-HP Tamel SG80-2A
PC-based Platforms	NI PXIe-1085, NI PXIe-1082
FPGA Modules	NI PXI-7854R, NI PXI-7855R
Transient Limiter	Agilent 11947A
Oscilloscope	LeCroy WaveMaster 804Zi-A

The only parameters changing in current study were converters' switching frequency (f_{ci}) and phase (θ_i) under unsynchronized condition. For synchronized condition the default values were 500 ns, 0.85 (modulation index), 50 Hz (modulating frequency - f_s) and 15 kHz (switching frequency - f_c) as in [18]. Then, for unsynchronized condition two operation modes were assessed: 1. carriers phase-shifted under f_{ci} at 15 kHz in FPGA controllers, i.e. $f_{c1} = f_{c2} = f_{c3} = f_{c4}$, $\theta_1 \neq \theta_2 \neq \theta_3 \neq \theta_4$, to demonstrate beat frequency and superposition effects on standing waves; 2. f_{ci} at different frequencies - i.e. $f_{c1} = 10\,\text{kHz}$, $f_{c2} = 15\,\text{kHz}$, $f_{c3} = 20\,\text{kHz}$, $f_{c4} = 30\,\text{kHz}$, to show frequency aggregation. Then, an EMI receiver measured the spectrum of conducted emissions by a quasi-peak (QP) detector. To accomplish it, EMI levels were assessed after applying input voltage of 200 V_{DC} to the inverters.

IV. RESULTS AND DISCUSSION

This section describes three case studies in different synchronization conditions and in different physical domains. The first case deals with frequency-domain analysis following the CISPR-16 in bands A and B. The second describes the time-frequency domain in low-frequency range showing the effects

into synchronization conditions. The third one is time-domain over the ground current in PE connection point among the variable speed drives. This experiment is especially interesting to assess the effect on the synchronization conditions over the grounding current when multiple devices are connected to point of common coupling (PCC).

A. Case Study 1 - Frequency-Domain on 9 kHz to 30 MHz

This case addresses the EMI in stand-alone and aggregated operation modes. Considering the IF filters adopted by the CISPR-16 for CISPR-A and CISPR-B bands, the spectrum for a variable speed drive gets harmonic components up to 150 kHz, then the shape gets wide-band for higher frequencies as seen in Fig. 2.
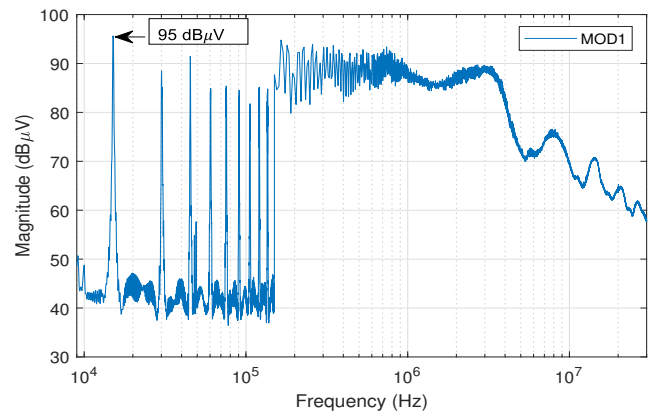

Fig. 2: Frequency spectrum for stand-alone mode.

In CISPR-A band, it exhibits narrow-band well-defined harmonic components due to the 200 Hz IF filter RBW, at maximum on 15 kHz, which is the default switching frequency (f_c) with 95 dBμV. Conversely, it shows a wide-band envelope for frequencies higher than 150 kHz due to the 9 kHz IF filter RBW, reaching 92 dBμV. As expected, those values surpass Group 1 and Class A CISPR 11 limits, due to high dv/dt and di/dt (coming from switching behavior, unbalanced voltages, parasitics and cables' resonances) since it has no EMI filters for the purpose of this study.

For multiconverters operation mode, the synchronized, unsynchronized with phase-shifting and unsynchronized with different frequencies conditions are represented in Fig. 3-A, -B and -C, respectively. In all charts the spectrum is overlapping each other to highlight the differences in-between. Each converter plus motor were dubbed "MOD" for module, to ease the description in the charts' legend.

The synchronized condition is shown in the first graph, Fig. 3-A. It presents an increasing EMI level which varies 11 dBμV - from 96 dBμV ($N = 1$, one converter) to 107 dBμV ($N = 4$, four converters). Another interesting effect is the increasing the background noise (noise floor) in 10 dBμV - from 40 dBμV ($N = 1$) to 50 dBμV ($N = 4$).

The phase-shifted unsynchronized frequency condition is shown in second graph (Fig.3-B). The EMI levels also increase with N, however it now shows 8 dBμV in difference, from 96 dBμV ($N = 1$) to 104 dBμV ($N = 4$). It also shows a raising
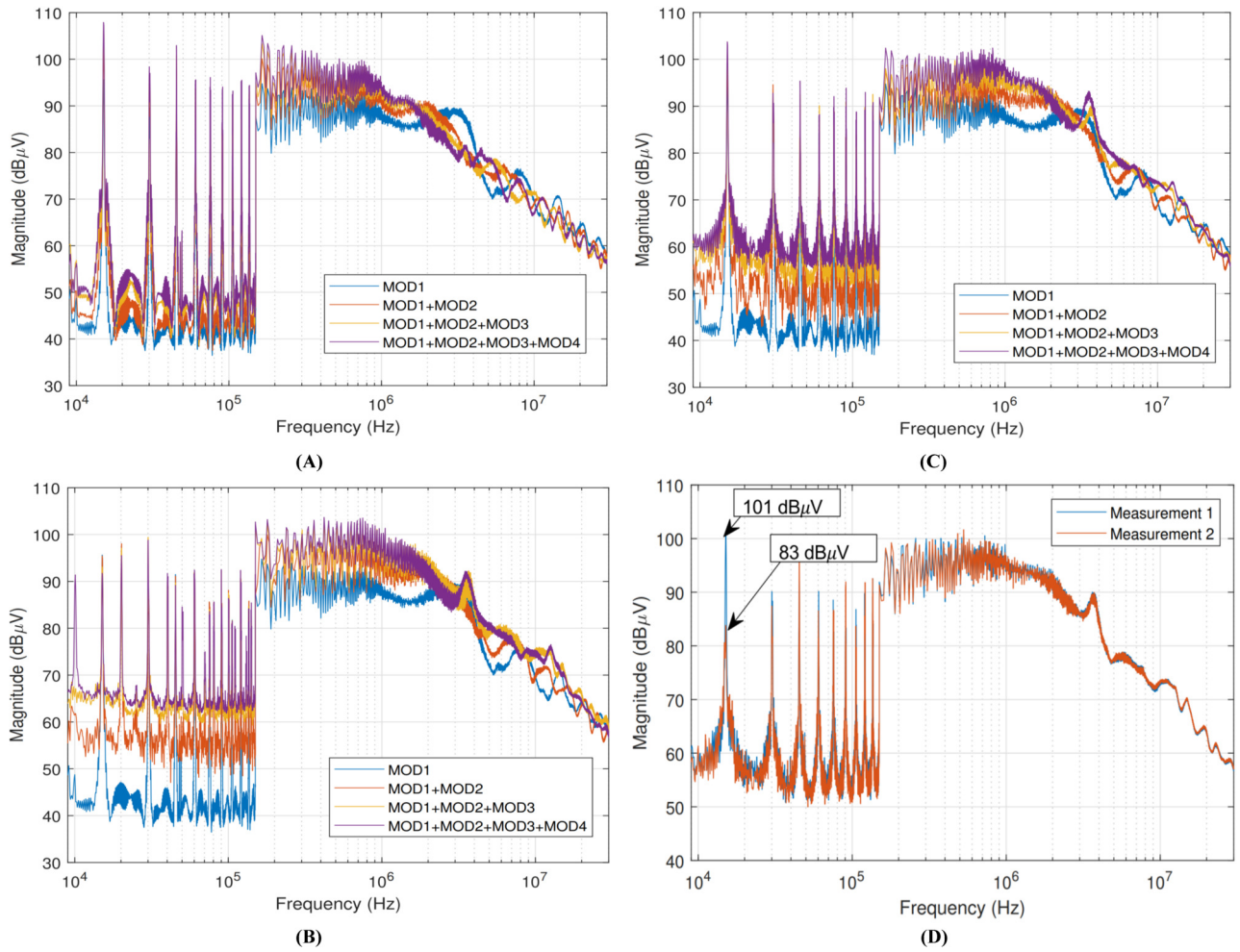
Fig. 3: Spectrum for synchronization conditions: (A) Synchronized converters. (B) Unsynchronized converters, phase-shifted f_{ci}. (C) Unsynchronized converters, different f_{ci}. (D) Two measurements done in the same setup settings at different time interval, underlining the issue with 2-D measurement.

in background noise but of 20 dBμV, from 40 dBμV ($N = 1$) to 60 dBμV ($N = 4$).

For unsyncronized with different switching frequency (Fig. 3-C), the comparison is not applicable since all the converters are running in different switching frequencies. However, the highest peak occurs on 99 dBμV - reducing 8 dBμV against highest peak in synchronized condition. Finally, it also presents increasing effect on noise floor of 25 dBμV, from 40 dBμV ($N = 1$) to 65 dBμV ($N = 4$).

Nevertheless, using 2D measurements is improper since it can led to misreading and imprecise results as shown in Fig. 3-D. It presents two measurements for three converters in the same setup and parameters, however with phase-shifted carriers, resulting in different EMI levels during time instants t_1 (curve in blue) and t_2 (curve in orange).

Those levels (Fig. 3-D) go from lowest (83 dBμV) to highest peak value (101 dBμV), resulting in 18 dBμV of difference. Since the highest values are below 1 MHz and an investigation in low frequency (below 150 kHz) in needed, the Section IV-B describes the time-frequency domain in which is possible to map the frequency variation along the time.

B. Case Study 2 - Time-Frequency-Domain on 9-150 kHz

The Fig. 4 shows EMI for synchronization conditions in spectrogram (time-frequency domain). Considering the values obtained from the spectrogram EMI peak values Fig. 4-(A), the EMI peak values for synchronized converters (Fig. 1, blue arrow) follow the theoretical-driven values with difference of 12 dB between $N = 4$ and $N = 1$. It can be said that the values for parallel drives in synchronized are directly proportional to the number of aggregated converters following (3), for synchronized condition.

The second synchronization condition, shown in Fig. 4-(B), describes the emission behavior for unsynchronized phase-shifted PWM with same switching frequency (centered at 15 kHz), in which each converter is signal-fed up by its own FPGA-based or PC-based device with default parameters (see Fig. 1, grey arrow). For $N > 1$, the EMI peaks are lower than in the synchronized condition, reaching maximum at $N = 3$ with 5 dB of difference. An important phenomenon, which starts at $N = 2$, is the beat frequency, in which the harmonic components superposition creates standing waves, due to the carriers waves moving in different directions (phase-
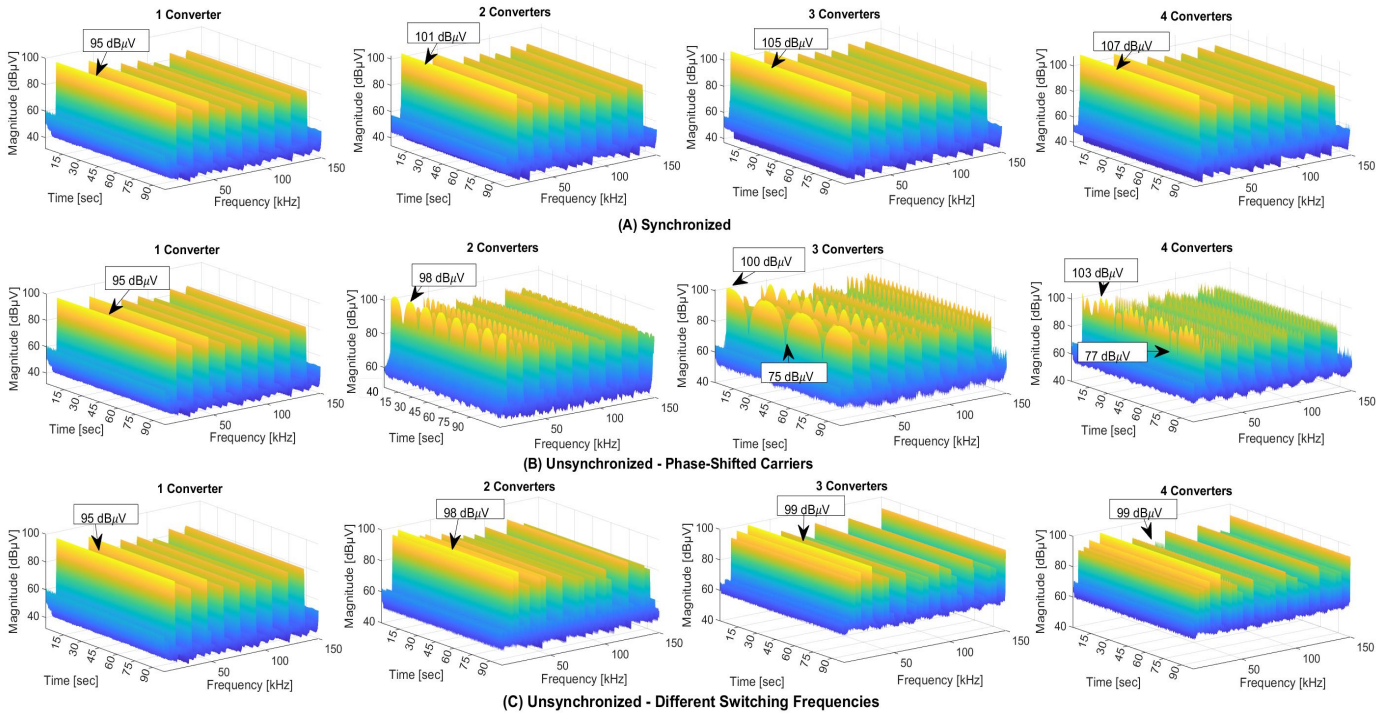
Fig. 4: EMI levels by increasing N in synchronization conditions on CISPR band A: (A) Synchronized; (B) Unsynchronized, phase-shifted f_{ci}; and (C) Unsynchronized with different f_{ci}.

shifted). This basically shows three things: 1. frequency-domain chart measurements can be subject to errors if not appropriately analyzed with in time-frequency-domain-based measurement technique; 2. More spikes are added to the bell shape as much as more inverters are being used, and; 3. The superposition (standing waves) also happens for all harmonics in the frequency range.

In the third case, Fig. 4-(C), the inverters are unsynchronized under different switching frequencies: (see Section for values). It is seen that the peaks increase with higher frequencies and the number of harmonics components also increases following the number of different frequencies. The EMI issues related are: (1) Harmonic pollution; (2) Frequency switching effects despite EMI peak levels decreased comparing with other synchronization conditions. All EMI peak values from unsynchronized conditions are below those for synchronized ones, reaching maximum of 8 dB at $N = 4$ (between synchronized and unsynchronized with different f_c conditions).

Giving that common-mode noise flows from the cables to the grounding, the PE cable current was taken as the next case study using time-domain analysis.

C. Case Study 3 - Time-Domain Analysis for Grounding Current

In Fig. 5 ground current for the system is shown, from oscilloscope at 250 MSa/s. In (A), the synchronized FPGA-clock for inverters produces a current of 124 mArms, with peaks ranging [-2.5, 2.09] A. Regarding (B), it shows unsynchronized tick-based (phase-shifted) inverters PWM reaching 72 mArms and, minimum and maximum peaks of - 84 mA

and 90 mA, respectively. Finally, on (C), it shows a current of 80 mArms and peaks between - 94 mA and 97 mA.
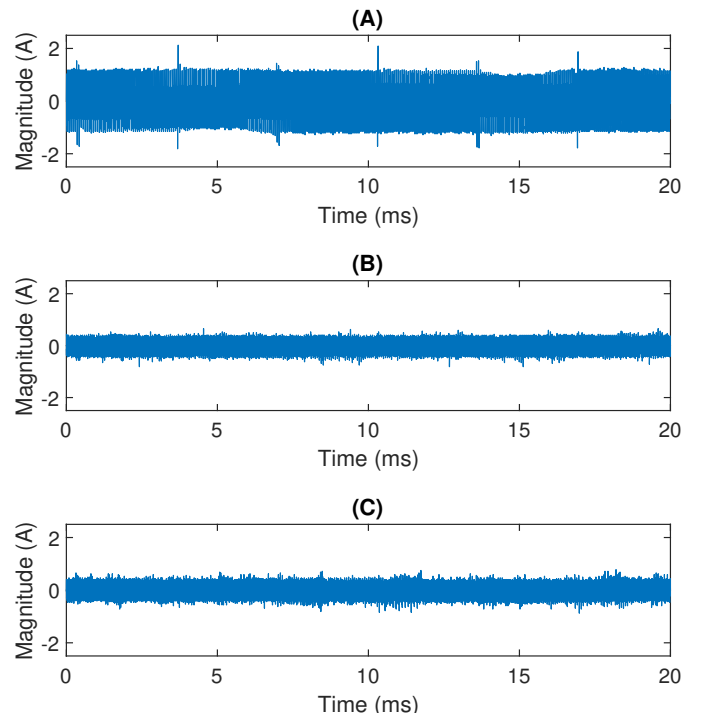

Fig. 5: Ground current at: (A) Synchronized; (B) Unsynchronized phase-shifted f_{ci}; (C) Unsynchronized at different f_{ci}.

Comparing the highest peaks in (A) with (B) and (C), the reduction in ground current peaks reaches 29 dB as follows

the equation in (4):

$$I_{dB} = 20 \times \log_{10}\left(\frac{I_{out}}{I_{in}}\right) \qquad (4)$$

It is emphasized that in ground current measurement, those relationships between ground current values and EMI can be particularly interesting for EMI assessment of electronic systems where a high number of converters are connected to PCC and when there is a progressive penetration of power electronics devices in distributed grids. Is noteworthy that there are several other PWM switching techniques to reduce the EMI peak levels (e.g. THPWM, DPWM and AZSPWM) using deterministic PWM techniques as shown in [11].

V. CONCLUSION

In this paper the frequency aggregation provided by multiple variable speed drives in different conditions of synchronization in a FPGA-driven testbench is investigated from 9 kHz to 30 MHz using multi-domain measurement technique. It is clear that more than one dimension technique is necessary to analyze a set of converters. In addition, that time-frequency-domain is preferable above single domain, especially for unsynchronized systems with phase-shifted carriers generating frequency beat phenomenon.

The influence of synchronization method on multiconverters systems related to the conducted emission is foregrounded. The synchronized converters emit the highest EMI level due harmonic current summation components at same phase (constructive interference). This is reflected to the grounding current, which is also high impacted by the harmonics in the multiconverters system and can be simply reduced providing different switching frequencies for each converter (avoiding harmonic constructive effect).

For further studies, EMI levels under different conditions of loads can be assessed and other techniques for harmonic decomposition can be used as an extension on the detailed analysis for frequency aggregation.

ACKNOWLEDGMENT

REFERENCES

[1] CENELEC, "Investigation Results on Electromagnetic Interference in the Frequency Range below 150 kHz - Irish Standard Recommendation, S.R. CLC/TR 50669:2017." Tech. Rep., 2018.

[2] Á. Espín-Delgado, "Propagation of Supraharmonics in Low-Voltage Networks Propagation of Supraharmonics in Low-Voltage Networks Propagation of Supraharmonics in Low-Voltage Networks," 2022.

[3] Á. Espín-Delgado, S. Rönnberg, S. Sudha Letha, and M. Bollen, "Diagnosis of supraharmonics-related problems based on the effects on electrical equipment," *Electric Power Systems Research*, vol. 195, jun 2021.

[4] L. Malburg, N. Moonen, and F. Leferink, "Superposition of EMI in multiple interconnected SMPS," in *2022 IEEE International Symposium on Electromagnetic Compatibility and Signal/Power Integrity, EMCSI 2022*. Institute of Electrical and Electronics Engineers Inc., 2022, pp. 362–367.

[5] W. E. Sayed, H. Loschi, A. Madi, N. Moonen, R. Smolenski, and F. Leferink, "Low-Frequency Envelope of DC/DC Converters due Differences in the Control Hardware Features," in *Proceedings of the 2021 Asia-Pacific International Symposium on Electromagnetic Compatibility, APEMC 2021*. IEEE, 2021.

[6] A. Moradi, F. Zare, D. Kumar, J. Yaghoobi, R. Sharma, and D. Kroese, "Current Harmonics Generated by Multiple Adjustable-Speed Drives in Distribution Networks in the Frequency Range of 2-9 kHz," *IEEE Transactions on Industry Applications*, vol. 58, no. 4, pp. 4744–4757, 2022.

[7] R. Smolenski, P. Lezynski, J. Bojarski, W. Drozdz, and L. C. Long, "Electromagnetic compatibility assessment in multiconverter power systems – Conducted interference issues," *Measurement: Journal of the International Measurement Confederation*, vol. 165, p. 108119, 2020. [Online]. Available: https://doi.org/10.1016/j.measurement.2020.108119

[8] J. Yaghoobi, A. Alduraibi, and F. Zare, "Current Harmonic Estimation Techniques based on Voltage Measurements in Distribution Networks; Current Harmonic Estimation Techniques based on Voltage Measurements in Distribution Networks," in *Australasian Universities Power Engineering Conference, AUPEC 2018*, 2018.

[9] Z. Zhang, Y. Hu, X. Chen, G. W. Jewell, and H. Li, "A Review on Conductive Common-Mode EMI Suppression Methods in Inverter Fed Motor Drives," *IEEE Access*, vol. 9, pp. 18 345–18 360, 2021.

[10] J. Hu, X. Xu, D. Cao, and G. Liu, "Analysis and optimization of electromagnetic compatibility for electric vehicles," *IEEE Electromagnetic Compatibility Magazine*, vol. 8, no. 4, pp. 50–55, 2019.

[11] D. Jiang, J. Chen, and Z. Shen, "Common mode EMI reduction through PWM methods for three-phase motor controller," *CES Transactions on Electrical Machines and Systems*, vol. 3, no. 2, pp. 133–142, 2019.

[12] B. Revol, J. Roudet, J. L. Schanen, and P. Loizelet, "EMI study of three-phase inverter-fed motor drives," *IEEE Transactions on Industry Applications*, vol. 47, no. 1, pp. 223–231, 2011.

[13] D. Grahame Holmes and Thomas A. Lipo, *Pulse Width Modulation for Power Converters: Principles and Practice*. IEEE Press, 2003.

[14] Y. Wang, Y. Xu, S. Tao, A. Siddique, and X. Dong, "A Flexible Supraharmonic Group Method Based on Switching Frequency Identification," *IEEE Access*, vol. 8, pp. 39 491–39 501, 2020.

[15] L. M. A. Aguilar, C. Robledo-Sánchez, M. L. A. Carrasco, and M. M. M. Otero, "The principle of superposition for waves: The amplitude and phase modulation phenomena," *Appl. Math. Inf. Sci*, vol. 6, no. 2, pp. 307–315, 2012. [Online]. Available: www.naturalspublishing.com/Journals.asp

[16] M. P. Knapp, "Sines and Cosines of Angles in Arithmetic Progression," *Mathematics Magazine*, vol. 82, no. 5, pp. 371–372, dec 2009.

[17] S. Greitzer, "Many cheerful facts," in *Arbelos*, 1986, pp. 14–17. [Online]. Available: https://matthew-brett.github.io/teaching/sums_of_cosines.html

[18] D. Nascimento, R. Smolenski, P. Lezynski, A. Matthee, N. Moonen, and F. Leferink, "Versatile LabVIEW-FPGA-based Testbench for Electromagnetic Interference Evaluation in VSDs," in *2022 International Symposium on Electromagnetic Compatibility*. Gothenburg: IEEE, 2022, pp. 1–6.

[19] H. Loschi, R. Smolenski, P. Lezynski, D. Nascimento, and G. Demidova, "Aggregated conducted electromagnetic interference generated by DC/DC converters with deterministic and random modulation," *Energies*, vol. 13, no. 14, 2020.